Inorg. Chem. **2003**, *42*, 6230–6240

Cyanide Adducts on the Diruthenium Core of $[Ru_2(L)_4]^+$ (L = ap, CH_3ap, Fap, or F_3ap). Electronic Properties and Binding Modes of the Bridging Ligand

John L. Bear,*,† Wei-Zhong Chen,‡ Boacheng Han,†,|| Shurong Huang,† Li-Lun Wang,† Antoine Thuriere,† Eric Van Caemelbecke,†,§ Karl M. Kadish,*,† and Tong Ren*,‡

Department of Chemistry, University of Houston, Houston, Texas 77204-5003, Department of Chemistry, University of Miami, Coral Gables, Florida 33146, and Department of Chemistry, Houston Baptist University, Houston, Texas 77074-3298

Received June 13, 2003

The products of the reaction between CN^- and four different diruthenium complexes of the type $Ru_2(L)_4Cl$ where L = 2-CH_3ap (2-(2-methylanilino)pyridinate anion), ap (2-anilinopyridinate anion), 2-Fap (2-(2-fluoroanilino)pyridinate anion), or 2,4,6-F_3ap (2-(2,4,6-trifluoroanilino)pyridinate anion) are reported. Mono- and/or dicyano adducts of the type $Ru_2(L)_4(CN)$ and $Ru_2(L)_4(CN)_2$ are found exclusively as reaction products when either the 2-CH_3ap or the ap derivative is reacted with CN^-, but diruthenium complexes with formulations of the type $Ru_2(F_xap)_3[\mu$-(*o*-NC)F_{x-1}-ap](μ-CN) or $Ru_2(F_xap)_4(\mu$-CN)$_2$ ($x = 1$ or 3) are also generated when $Ru_2(Fap)_4Cl$ or $Ru_2(F_3ap)_4Cl$ is reacted with CN^-. More specifically, four products formulated as $Ru_2(Fap)_4(CN)$, $Ru_2(Fap)_4(CN)_2$, $Ru_2(Fap)_3[\mu$-(*o*-NC)ap](μ-CN), and $Ru_2(Fap)_4(\mu$-CN$)_2$ can be isolated from a reaction of CN^- with the Fap derivative, but the exact type and yield of these compounds depend on the temperature at which the experiment is carried out. In the case of the F_3ap derivative, the only diruthenium complex isolated from the reaction mixture has the formulation $Ru_2(F_3ap)_3[\mu$-(*o*-NC)F_2ap](μ-CN) and this compound has structural, electrochemical, and spectroscopic properties quite similar to that of previously characterized $Ru_2(F_5ap)[\mu$-(*o*-NC)F_4ap](μ-CN). Both the mono- and dicyano derivatives synthesized in this study possess the isomer type of their parent chloro complexes. The Ru–Ru bond lengths of $Ru_2(ap)_4(CN)$ and Ru_2(2-CH_3ap)$_4$(CN) are longer than those of $Ru_2(ap)_4Cl$ and $Ru_2(CH_3ap)_4Cl$, respectively, and this is accounted for by the strong σ-donor properties of the CN^- ligand as compared to Cl^-. The Ru–C bonds in $Ru_2(ap)_4(CN)_2$ are significantly shorter than those in $Ru_2(ap)_4(CN)$, thus revealing a greatly enhanced Ru–CN interaction in the dicyano adduct, a result which is also indicated by the fact that ν_{CN} in $Ru_2(ap)_4(CN)_2$ is 50 cm^{-1} higher than ν_{CN} in Ru_2-(ap)$_4$(CN). Although both (4,0) $Ru_2(ap)_4(CN)_2$ and (3,1) $Ru_2(Fap)_4(CN)_2$ possess the same formulation, there are clear structural differences between the two complexes and this can be explained by the fact that the two cyano derivatives possess a different binding symmetry of the bridging ligands. Each mono- and dicyano adduct was electrochemically investigated in CH_2Cl_2 containing TBAP as supporting electrolyte. $Ru_2(ap)_4(CN)$, $Ru_2(CH_3ap)_4$-(CN), and $Ru_2(Fap)_4(CN)$ undergo one reduction and two oxidations. The two dicyano adducts of the ap and Fap derivatives are characterized by two reductions and one oxidation. The potentials of these processes are all negatively shifted in potential by 400–720 mV with respect to half-wave potentials for the same redox couples of the monocyano derivatives, with the exact value depending upon the specific redox reaction.

Introduction

Recent years have witnessed a rapid development in utilizing dimetallic paddlewheel complexes as synthons for supramolecules.[1–3] Notably, Cotton and co-workers have realized molecular triangles, squares, cages, and loops based on connecting Mo_2/Rh_2 units at either equatorial or axial positions.[1,2] Work from the laboratories of Cotton,[4,5] Dunbar,[6,7] Kühn,[8–10] Bear,[11] and Ren[12,13] has demonstrated that

* Authors to whom correspondence should be addressed. E-mail: kkadish@uh.edu.
† University of Houston.
‡ University of Miami.
|| Current address: Department of Chemistry, University of Wisconsin—Whitewater, Whitewater, WI 53190.
§ Houston Baptist University.

(1) Cotton, F. A.; Lin, C.; Murillo, C. A. *Acc. Chem. Res.* **2001**, *34*, 759.
(2) Cotton, F. A.; Lin, C.; Murillo, C. A. *Proc. Natl. Acad. Sci., U. S. A.* **2002**, *99*, 4810.
(3) Wong, K.-T.; Lehn, J.-M., Peng, S.-M.; Lee, G.-H. *Chem. Commum.* **2000**, 2259.

10.1021/ic030195m CCC: $25.00
Published on Web 09/03/2003

electron-rich Ru_2 and Rh_2 units form both linear arrays and 2-D nets through axial coordination of di- and tetratopic linkers. Among potential ditopic linkers is the cyano (CN^-) ligand, which is especially interesting due to its ability to mediate strong spin−spin couplings.[14,15] Recently, metal−cyano complexes have been used as N-donor ligands at Ru_2 centers to form both extended arrays[16,17] and molecular complexes.[18]

Diruthenium complexes supported by N,N′-bidentate ligands exhibit rich redox activities and magnetic properties, and their axial cyano adducts could become unique building blocks. Bear and co-workers[19] have demonstrated that $Ru_2(dpf)_4$ (dpf = diphenylformamidinate) readily forms both mono- and dicyano adducts, and the latter was carefully characterized. The structure of $Ru_2(dpf)_4(CN)_2$ demonstrates that the aryl groups flanking both axial positions prevent the coordinated CN^- groups from functioning as N-donor ligands.

In contrast to $Ru_2(dpf)_4Cl$, the reaction between $Ru_2(F_5ap)_4Cl$ (F_5ap = 2-pentafluoroanilinopyridinate) and NaCN under reflux conditions affords three dicyano products where the cyano ligands are all in bridging modes.[20] Nothing has been published on the reactions of CN^- with other known Ru_2 complexes containing ap or substituted ap bridging ligands, and we now report that by controlling the reaction conditions, both mono- and dicyano adducts on the $Ru_2(ap)_4$ and $Ru_2(Fap)_4$ core can be preferentially synthesized where the CN^- ligands are axially coordinated in both cases. The difference in the coordination mode of CN^- ligands between the Ru_2 complexes of ap (axial) and F_5ap (μ-C) is likely attributed to the labile nature of F_5ap ligand, which is clearly a consequence of perfluorination on the aniline ring. Naturally, one would be intrigued about the reactivity toward CN^- ligands by the Ru_2 complexes with ligands of medium basicity, i.e., partially fluorinated ap anions Fap and F_3ap. Reactions between CN^- and $Ru_2(F_xap)_4Cl$ (x = 1 or 3) and characterizations of products isolated from these reactions are also reported.

Experimental Section

General Remarks. Potassium cyanide and sodium cyanide were purchased from Aldrich, tetra-*n*-butylammonium perchlorate (TBAP) was purchased from Fluka, and silica gel was purchased from Merck or Aldrich. THF was distilled over Na/benzophenone under an N_2 atmosphere prior to use. Absolute dichloromethane (water content <0.005%, sealed under nitrogen) was purchased from Fluka and used as received for the electrochemical measurements. Potassium bromide was purchased from International Crystal Laboratories and was stored at 40 °C in a vacuum oven prior to use.

^{1}H NMR spectra were recorded on a Bruker AVANCE300 NMR spectrometer with chemical shifts (δ) referenced to the residual $CHCl_3$. IR spectra were recorded on a Perkin-Elmer 2000 FTIR spectrometer or a FTIR Nicolet 550 Magna-IR spectrometer using KBr disks. UV−vis spectra were obtained with a Perkin-Elmer Lambda-900 UV−vis spectrophotometer or a Hewlett-Packard model 8453 diode array spectrophotometer. Magnetic susceptibility was measured at 298 K with a Johnson Matthey Mark-I magnetic susceptibility balance or was determined by the Evan's method.[21,22] Electron spin resonance (ESR) spectra were recorded on a Bruker ER 100E spectrometer. The g values were measured with respect to diphenylpicrylhydrazyl (DPPH, $g = 2.0036 \pm 0.0003$). Mass spectra were recorded on a Finnigan TSQ 700 instrument at the University of Texas, Austin. Standard fast atom bombardment was used, and *m*-nitrobenzyl alcohol (NBA) was used as the liquid matrix.

Cyclic voltammograms were obtained using an EG&G Princeton Applied Research (PAR) model 173 potentiostat/galvanostat or an IBM model EC 225 voltammetric analyzer using a three-electrode system which consisted of a platinum button (1.0 mm diameter) or a glassy carbon working electrode (3.0 mm diameter), a platinum wire counter electrode, and a homemade saturated calomel reference electrode (SCE) as the reference electrode. The SCE was separated from the bulk of the solution by a fritted-glass bridge of low porosity that contained the solvent/supporting electrolyte mixture. TBAP (0.1 M) was used as the supporting electrolyte for the cyclic voltammetric measurements. The ferrocenium/ferrocene couple in CH_2Cl_2, 0.1 M TBAP was observed at 0.49 V vs SCE under our experimental conditions.

Synthesis of Starting Compounds. $Ru_2(ap)_4Cl$,[23] $Ru_2(CH_3ap)_4Cl$,[24] $Ru_2(Fap)_4Cl$,[25] and $Ru_2(F_3ap)_4Cl$[24] were prepared as described in the literature.

Synthesis of (4,0) $Ru_2(ap)_4(CN)$ (1). Potassium cyanide (15 mg, 0.23 mmol) in 5 mL of methanol was added to a THF solution of $Ru_2(ap)_4Cl$ (200 mg, 0.22 mmol in 40 mL), and the mixture was stirred under argon while the progress was monitored by thin-layer chromatography (TLC). Upon the complete disappearance of $Ru_2(ap)_4Cl$ (ca. 2 h), the reaction mixture was filtered through a 2-cm silica gel pad deactivated with Et_3N. Solvent removal from the filtrate resulted in a green solid which was recrystallized from THF/hexanes to afford **1** as green microcrystals. Yield: 181 mg, (91% based on Ru). R_f (v/v/v, CH_2Cl_2/hexanes/triethylamine = 3/6/1), 0.85. UV−vis [λ_{max}, nm (ϵ, M^{-1} cm^{-1})]: 462 (4410), 763 (5800). IR, ν(C≡N)/cm^{-1}: 2038 (s). MS-FAB (*m*/*e*, based on ^{101}Ru): 906 [MH^+]. χ_{mol}(corrected) = 5.64×10^{-3} emu, μ_{eff} = 3.67 μ_B.

(4) Cotton, F. A.; Kim, Y. *J. Am. Chem. Soc.* **1993**, *115*, 8511.
(5) Cotton, F. A.; Kim, Y.; Ren, T. *Inorg. Chem.* **1992**, *31*, 2723.
(6) Miyasaka, H.; Campos-Fernández, C. S.; Clérac, R.; Dunbar, K. R. *Angew. Chem., Int. Ed. Engl.* **2000**, *39*, 3831.
(7) Miyasaka, H.; Clérac, R.; Campos-Fernández, C. S.; Dunbar, K. R. *Inorg. Chem.* **2001**, *40*, 1663.
(8) Zuo, J.-L.; Herdtweck, E.; Kühn, F. E. *J. Chem. Soc., Dalton Trans.* **2002**, 1244.
(9) Zuo, J.-L.; Herdtweck, E.; Biani, F. F. D.; Santos, A. M.; Kühn, F. E. *New J. Chem.* **2002**, *26*, 889.
(10) Zuo, J.-L.; Biani, F. F. d.; Santos, A. M.; Köhler, K.; Kühn, F. E. *Eur. J. Inorg. Chem.* **2003**, 449.
(11) Bear, J. L.; Han, B.; Wu, Z.; Caemelbecke, E. V.; Kadish, K. M. *Inorg. Chem.* **2001**, *40*, 2275.
(12) Ren, T.; Xu, G. *Comments Inorg. Chem.* **2002**, *23*, 355.
(13) Ren, T.; Zou, G.; Alvarez, J. C. *Chem. Commun.* **2000**, 1197.
(14) Dunbar, K. R.; Heintz, R. A. *Prog. Inorg. Chem.* **1997**, *45*, 283.
(15) Miller, J. S.; Manson, J. L. *Acc. Chem. Res.* **2001**, *34*, 563.
(16) Liao, Y.; Shum, W. W.; Miller, J. S. *J. Am. Chem. Soc.* **2002**, *124*, 9336.
(17) Yoshioka, D.; Mikuriya, M.; Handa, M. *Chem. Lett.* **2002**, 1044.
(18) Zhang, L.-Y.; Chen, J.-L.; Shi, L.-X.; Chen, Z.-N. *Organometallics* **2002**, *21*, 5919.
(19) Bear, J. L.; Han, B.; Huang, S.; Kadish, K. M. *Inorg. Chem.* **1996**, *35*, 3012.
(20) Bear, J. L.; Li, Y.; Cui, J.; Han, B.; Caemelbecke, E. V.; Phan, T.; Kadish, K. M. *Inorg. Chem.* **2000**, *39*, 857.
(21) Evans, J. *J. Chem. Soc.* **1959**, 2003.
(22) Loliger, J.; Scheffold, R. *J. Chem. Educ.* **1972**, *49*, 646.
(23) Chakravarty, A. R.; Cotton, F. A.; Tocher, D. A. *Inorg. Chem.* **1985**, *24*, 172.
(24) Kadish, K. M.; Wang, L.-L.; Thuriere, A,; Van Caemelbecke, E.; Bear, J. L. *Inorg. Chem.* **2003**, *42*, 834.
(25) Bear, J. L.; Wellhoff, J.; Royal, G.; Van Caemelbecke, E.; Eapen, S.; Kadish, K. M. *Inorg. Chem.* **2001**, *40*, 2282.

Synthesis of $Ru_2(ap)_4(CN)_2$ (2). Potassium cyanide (150 mg, 2.2 mmol) dissolved in 10 mL of methanol was added to a CH_2Cl_2 solution of $Ru_2(ap)_4Cl$ (200 mg, 0.22 mmol in 50 mL), and the solution was stirred with concurrent air bubbling for 6 h, during which the color of the reaction mixture changed from green to royal blue. The reaction mixture was washed with a copious amount of water to remove excess KCN. Solvent removal from the organic phase yielded a purple solid, which was purified via silica column chromatography to afford both **2** as the major product (130 mg, 63%) and **1** as the minor product. $R_f = 0.65$. UV−vis [λ_{max}, nm (ϵ, M^{-1} cm^{-1})]: 568 (3640), 996 (4060). IR, ν(C≡N)/cm^{-1}: 2095 (m), 2082 (m). MS-FAB (*m*/*e*, based on ^{101}Ru): 905 [$M^+ - CN$]. ^1H NMR ($CDCl_3$): 9.18−8.99 (m, 4H, aromatic), 7.66−6.76 (m, 16H, aromatic), 6.98−6.56 (m, 8H, aromatic), 5.56 (m, 8H, aromatic).

Synthesis of (4,0) $Ru_2(CH_3ap)_4(CN)$ (3). The title compound was synthesized following a procedure similar to the one used for the reaction between $Ru_2(F_5ap)_4Cl$ and NaCN.[20] $Ru_2(CH_3ap)_4Cl$ (100 mg, 0.10 mmol) was dissolved in 100 mL of fresh anhydrous THF prior to addition of excess NaCN (90 mg, 1.84 mmol). The reaction mixture was refluxed at 70 °C in air for 48 h. The color of the solution remained green for the whole time the experiment was carried out. The solvent was removed under vacuum, after which the excess NaCN was removed from the reaction mixture by extraction with H_2O. The organic layer was dried over $MgSO_4$ before removing the solvent by rotary evaporation. The compound was purified on a silica gel column using acetone/*n*-hexane (3:7 v/v) as eluent and was recovered in a 55% yield. MS (*m*/*e*, fragment): 961 $[Ru_2(CH_3ap)_4CN]^+$. UV−vis [λ_{max}, nm ($\epsilon \times 10^{-3}$, M^{-1} cm^{-1})]: 463 (2.8), 756 (4.3).

Synthesis of $Ru_2(Fap)_4(CN)$ (4), $Ru_2(Fap)_4(CN)_2$ (5), $Ru_2(Fap)_3[\mu$-(*o*-NC)ap$](\mu$-CN) (6), and $Ru_2(Fap)_4(\mu$-$CN)_2$ (7). All four compounds were isolated during the reaction between the (3,1) isomer of $Ru_2(Fap)_4Cl$ (50 mg, 0.051 mmol) and NaCN (10 mg, 0.20 mmol) in 30 mL of fresh distilled THF under two different experimental conditions, but the exact type of diruthenium complex and its yield varied drastically with the experimental conditions. In both experiments, the reaction mixtures were left open to the atmosphere but in one case the reflux was done at room temperature while in the other it was carried out at 70 °C. Two bands (dark green and blue) were observed in the column when the reaction was carried at room temperature while three bands (green, blue, and green-blue) were found from the reaction at 70 °C. $Ru_2(Fap)_4(CN)_2$ **5** was obtained from reactions at both room temperature and 70 °C, but $Ru_2(Fap)_3[\mu$-(*o*-NC)ap$)](\mu$-CN) **6** was obtained only from the reaction at 70 °C. Compound **6** was isolated from the green band after it was subjected to column chromatography using a column packed with silica gel and 100% CH_2Cl_2 as eluent (yield 4%). Compound **5** was isolated from the blue band after it was subjected to column chromatography several times using CH_2Cl_2/hexanes (1:9 v/v) as eluent. The yield of **5** was 23 and 12% from the room temperature and 70 °C reactions, respectively.

Two other compounds were isolated during workup of the column (at room temperature and 70 °C) but no crystal structure could be obtained to confirm their formulation; one was obtained during purification of the dark green fraction while the other was isolated from the green-blue fraction. On the basis of their electrochemical behavior and mass spectral data, we formulate the dark green compound as $Ru_2(Fap)_4(CN)$ (**4**) and the blue-green product as $Ru_2(Fap)_4(\mu$-$CN)_2$ (**7**).

4. MS (*m*/*e*, fragment): 978 $[Ru_2(Fap)_4CN]^+$.

5. UV−vis [λ_{max}, nm ($\epsilon \times 10^{-3}$, M^{-1} cm^{-1})]: 457 (sh, 2.63), 564 (5.47), 669 (sh, 4.95), and 862 (5.19) nm (sh: shoulder peak). MS (*m*/*e*, fragment): 1002 $[Ru_2(Fap)_4(CN)_2]^+$. IR (KBr pellet): 2093 (m, b), 2080 (m, b), 1608 (s), 1489 (s), 1464 (s), 1421 (s), 1342 (m), 1292 (m), 1241 (s), 1196 (m), 1162 (w), 1105 (m), 1032 (w), 942 (w), 891 (w), 840 (w), 795 (w), 756 (m), 722 (w), 670 (w), 643 (w) cm^{-1}.

6. UV−vis, λ_{max} (nm): 677 and 808. IR (KBr pellet): 1976 (m), 1736 (s), 1538 (m, b), 1434 (s), 1366(s), 1220 (s), 1012 (m, b), 911 (m), 843 (m, b), 771 (m), 685 (m, b), 522 (s) cm^{-1}.

7. UV−vis, λ_{max} (nm): 703 and 974. MS (*m*/*e*, fragment): 1003 $[Ru_2(Fap)_4(\mu$-$CN)_2]^+$. IR (KBr pellet): 2045 (m), 1720(s), 1607 (s), 1494 (m) 1460 (s), 1379 (m), 1271 (m), 1192 (m) 1103 (s), 1023 (m), 847 (m), 804 (m), 754 (s), 713 (m), 622(m) cm^{-1}.

Synthesis of $Ru_2(F_3ap)_3[\mu$-(*o*-NC)F_2ap$](\mu$-CN) (8). This compound was obtained by reacting the (3,1) isomer of $Ru_2(F_3ap)_4Cl$ (100 mg, 0.089 mmol) with sodium cyanide (18 mg, 0.37 mmol) in 50 mL of fresh distilled THF. The reaction mixture was left open to the atmosphere while being refluxed overnight. The solution was dark green in the beginning and then gradually changed to dark blue. The solution was left to evaporate under the hood, after which it was extracted using CH_2Cl_2 and water. The organic layer was collected and evaporated under the hood. The remaining dark blue residue was purified on a silica gel column using 100% CH_2Cl_2 as the eluent. Three bands (green, purple, and blue) were observed in the column, but only the green fraction could be isolated. The title compound was obtained by slow evaporation of this fraction with a yield of 26%. This yield increased to 44% when the reaction was carried out at 70 °C. UV−vis [λ_{max}, nm ($10^{-3}\epsilon$, mol^{-1} L cm^{-1})]: 674 (4.37) and 795 (6.95). MS (*m*/*e*, fragment): 1128 $[Ru_2(F_3ap)_3[\mu$-(*o*-NC)F_2ap$)](\mu$-CN)$]^+$. IR (KBr pellet): 1993 (m), 1703 (m), 1600 (s), 1512 (s), 1466 (s), 1445 (s), 1424 (s), 1326 (m), 1305 (w), 1264 (m), 1207 (m), 1119 (s), 1031 (s), 860 (w), 855 (w), 824 (w), 813 (w), 754 (m), 731 (w) cm^{-1}.

Attempt to Rearrange 2. Compound **2** (50 mg) and 10-fold KCN dissolved in 20 mL of THF were refluxed in air. After overnight reflux, **1** was detected as the major product, and some unidentified compounds were found near the baseline of TLC plate. Reflux of **2** without KCN gave similar results.

Structural Determination of Compounds 1−3, 5, and 8. Single crystals of the five structurally characterized compounds were grown as follows: slow evaporation of a saturated THF solution (**1**), slow diffusion of methanol into CH_2Cl_2 solution (**2**), slow evaporation of a CH_2Cl_2 solution containing 0.1 M TBAP (**3**), or slow diffusion of *n*-hexane into a CH_2Cl_2 solution (**5** and **8**). The X-ray intensity data were measured using Mo Kα ($\lambda = 0.71073$ Å) either at 300 K on a Bruker SMART1000 CCD-based X-ray diffractometer system (**1** and **2**) or at 223 K on a Siemens SMART platform diffractometer equipped with a 1K CCD area detector (**3**, **5**, and **8**). For X-ray crystallographic analysis, crystals of dimension 0.49 × 0.27 × 0.03 mm^3 (**1**) and 0.25 × 0.21 × 0.05 mm^3 (**2**) were mounted in quartz capillaries with mother liquors, and crystals of dimension 0.40 × 0.12 × 0.25 mm (**3**), 0.40 × 0.40 × 0.06 mm^3 (**5**), and 0.20 × 0.18 × 0.16 mm^3 (**8**) were mounted on quartz fiber and placed in a steam of dry nitrogen gas at −50 °C. Data were measured using omega scans of 0.3° per frame such that a hemisphere (1271 frames) was collected. No decay was indicated for any of five data sets by the re-collection of the first 50 frames at the end of each data collection. The frames were integrated with the SAINT software package[26] using a narrow-frame integration algorithm, which also corrects for the Lorentz and polarization effects. Absorption corrections were applied using SADABS supplied by George Sheldrick.

The structures were solved and refined using the SHELXTL (Version 5.1) software package in the space groups $P\bar{1}$ for crystals **1**, **2**, and **8**; *C*2/*c* for **3**; and $P2_1/c$ for **5**. Positions of all

Table 1. Crystal Data for Compounds **1**−**3**, **5**, and **8**

	1·2THF·H_2O	**2**·CH_2Cl_2·MeOH	**3**·2CH_2Cl_2	**5**·CH_2Cl_2	**8**·0.5CH_2Cl_2·0.5C_6H_{14}
chemical formula	$C_{53}H_{54}N_9O_3Ru_2$	$C_{48}H_{42}Cl_2N_{10}ORu_2$	$C_{51}H_{48}N_9Ru_2Cl_4$	$C_{47}H_{34}N_{10}F_4Ru_2Cl_2$	$C_{48}H_{28}N_{10}F_{11}Ru_2Cl_{0.5}$
formula weight	1067.2	1048.0	1130.92	1087.88	1170.67
space group	$P\bar{1}$	$P\bar{1}$	$C2/c$	$P2_1/c$	$P\bar{1}$
a, Å	10.010(6)	16.378(4)	19.2291(7)	16.708(1)	16.2682(9)
b, Å	13.705(10)	16.456(4)	15.6453(5)	15.5031(9)	16.7828(9)
c, Å	19.698(16)	17.651(4)	17.4068(6)	17.046(1)	17.1006(9)
α, deg	74.01(8)	73.140(4)			88.568(1)
β, deg	79.31(8)	89.864(4)	108.710(1)	97.861(1)	88.568(1)
γ, deg	86.68(7)	89.870(5)			83.802(1)
V, Å^3	2553(3)	4553(2)	4960.0(3)	4374.0(4)	4637.8(4)
Z	2	4	4	4	4
T, °C	27	27	−50	−50	−50
λ(Mo Kα), Å	0.71073	0.71073	0.71073	0.71073	0.71073
ρ_{calc}, g cm^{-3}	1.388	1.529	1.514	1.652	1.677
μ, cm^{-1}	0.642	0.830	0.870	0.878	0.772
R	0.069	0.053	0.029	0.030	0.030
wR2	0.202	0.151	0.076	0.083	0.086

non-hydrogen atoms of diruthenium moieties were revealed by direct method. In the case of crystal **1**, the asymmetric unit contains one diruthenium molecule, one water molecule, and two THF molecules. In the case of **2**, the asymmetric unit contains two independent diruthenium molecules, two methanol, and two dichloromethane solvent molecules. The asymmetric unit of **3** consists of one-half molecule that is related to the other half by a crystallographic axis coincident with the Ru1−Ru2−C25 vector plus one molecule of methylene chloride solvent. The asymmetric unit of **5** consists of one diruthenium molecule and one molecule of methylene chloride solvent. Each of the four fluorine atoms in **5** is disordered over two different ortho carbon sites and was refined with occupancy constraint. The asymmetric unit of **8** contains two independent diruthenium molecules plus solvent molecules (one CH_2Cl_2 and one hexane). With all non-hydrogen atoms being anisotropic and all hydrogen atoms in calculated position and riding mode, the structure was refined to convergence by least-squares method on F^2, SHELXL-93, incorporated in SHELXTL.PC V 5.03.[27−29] Relevant information on the data collection and the figures of merit of final refinement are listed in Table 1.

Results and Discussion

Reaction between $Ru_2(ap)_4Cl$ and CN^-. $Ru_2(ap)_4Cl$ in THF readily undergoes a metathesis reaction with 1 equiv of KCN in an inert atmosphere to afford the monocyano adduct $Ru_2(ap)_4(CN)$ (**1**) in nearly quantitative yield (see Scheme 1). It was noted in previous syntheses of $Ru_2(dpf)_4$- and $Ru_2(ap)_4$-alkynyl compounds that the presence of excess LiCCZ under anaerobic conditions always yielded a solution whose color was significantly different from that of the monoalkynyl adduct,[19,30−32] and this was interpreted as due to the high tendency for formation of $[Ru_2(C_2Y)_2]^-$ in the absence of O_2. To our surprise, the addition of KCN in large excess to a solution of $Ru_2(ap)_4Cl$ *under argon* did not result in the appearance of any new product other than **1**.

Scheme 1. Mono-(1) and Bis-cyano (2) Complexes of $[Ru_2(ap)_4]$ Core

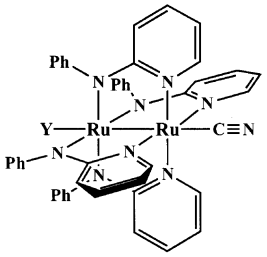

1, Y = none; **2**,Y = CN^-

Scheme 2. Formation of Mono- and Dicyano Adducts on $Ru_2(ap)_4$

$$[Ru_2]Cl \xrightarrow[-\ KCl]{1\ eq.\ KCN} [Ru_2](CN) \underset{}{\overset{excess\ CN^-}{\rightleftharpoons}} \{[Ru_2](CN)_2\}^- \xrightarrow{O_2} [Ru_2](CN)_2$$

Nevertheless, continuous air bubbling through this solution over an extended period of time led to a gradual shift in the solution color from green to deep purple. TLC analysis revealed a buildup of the new purple product which was separated from the residual **1** by column chromatography and identified as the dicyano adduct, **2** (see Scheme 2). The difference in reaction products involving the cyano and alkynyl ligands is likely due to the lower affinity of the CN^- ligand toward the $Ru_2(ap)_4$ core. Hence, the overwhelmingly predominant species produced from $Ru_2(ap)_4Cl$ under anaerobic conditions is $Ru_2(ap)_4(CN)$, while $\{Ru_2(ap)_4(CN)_2\}^-$ is only formed in trace amounts (which is undetected by TLC). Aerobic oxidation of the anionic CN^- complex to $Ru_2(ap)_4(CN)_2$ facilitates a shift of the equilibrium toward the neutral dicyano adduct formation and eventually resulted in **2** as the major product, as shown in Scheme 2. The coexistence of mono- and dicyano adducts was also noted in the reaction between $Ru_2(dpf)_4Cl$ and excess NaCN.[19]

Isolation of bridging dicyano complexes from refluxing $Ru_2(F_5ap)_4Cl$ with CN^- [20] prompted us to examine the possible formation of a *μ*-cyano-$Ru_2(ap)_4$ product. However, further reflux of **2** with or without KCN only led to its decomposition, giving **1** (major) and very polar unidentified products (minor) that were immobilized on silica TLC plate.

Compound **1** is paramagnetic and has an effective magnetic moment of 3.67 μ_B, indicating an $S = {}^3/_2$ ground state that is common to all $Ru_2(ap)_4L_{ax}$ compounds (L_{ax} is a

(26) *SAINT V 6.035 Software for the CCD Detector System* 1999 Bruker-AXS Inc.
(27) *SHELXTL 5.03 (WINDOW−NT Version), Program library for Structure Solution and Molecular Graphics* 1998 Bruker-AXS Inc.
(28) Sheldrick, G. M. *SHELXS-90, Program for the Solution of Crystal Structures*; University of Göttigen: Göttigen, Germany, 1990.
(29) Sheldrick, G. M. *SHELXL-93, Program for the Refinement of Crystal Structures*; University of Göttigen: Göttigen, Germany, 1993.
(30) Xu, G.; Ren, T. *Organometallics* **2001**, *20*, 2400.
(31) Ren, T. *Organometallics* **2002**, *21*, 732.
(32) Xu, G.; Ren, T. *J. Organomet. Chem.* **2002**, *655*, 239.

Table 2. Reaction Products between $Ru_2(L)_4Cl$ and Cyanide (L = ap, CH_3ap, Fap, F_3ap, or F_5ap)

		cyano adducts		
isomer type	bridging ligand, L	mono-CN	bis-CN	rearranged cyano products
(4,0)	ap	$Ru_2(ap)_4(CN)$ (**1**)	$Ru_2(ap)_4(CN)_2$ (**2**)	
(4,0)	CH_3ap	$Ru_2(CH_3ap)_4(CN)$ (**3**)		
(3,1)	Fap	$Ru_2(Fap)_4(CN)$ (**4**)	$Ru_2(Fap)_4(CN)_2$ (**5**)	$Ru_2(Fap)_3[\mu$-(*o*-NC)ap$](\mu$-CN) (**6**) $Ru_2(Fap)_4(\mu$-CN$)_2$ (**7**)
(3,1)	F_3ap			$Ru_2(F_3ap)_4[\mu$-(*o*-NC)F_2ap$](\mu$-CN) (**8**)
(3,1)	F_5ap[a]			$Ru_2(F_5ap)_3[\mu$-(*o*-NC)F_4ap$](\mu$-CN) $Ru_2(F_5ap)_4(\mu$-CN$)_2$ (2 isomers)

[a] Taken from ref 20.

monoanionic axial ligand). Similar to the $Ru_2(ap)_4(C_2Y)_2$ type complexes, compound **2** is diamagnetic, which facilitates its NMR characterization.

Reaction between $Ru_2(L)_4Cl$ and CN^- where L = CH_3ap, Fap, or F_3ap. Table 2 summarizes the type of diruthenium complexes obtained when reacting either the (3,1) or (4,0) isomer of $Ru_2(L)_4Cl$ with CN^-. The product isolated when reacting (3,1) $Ru_2(F_3ap)_4Cl$ and NaCN is $Ru_2(F_3ap)_3[\mu$-(*o*-NC)F_2ap$](\mu$-CN) (**8**) regardless of whether the reaction is carried out at room temperature or at 70 °C. In contrast, $Ru_2(Fap)_3[\mu$-(*o*-NC)ap$](\mu$-CN) (**6**) is isolated only when the reaction between NaCN and (3,1) $Ru_2(Fap)_4Cl$ is carried out at 70 °C. Indeed, at room temperature, this reaction gives $Ru_2(Fap)_4(CN)$ (**4**), $Ru_2(Fap)_4(CN)_2$ (**5**), and $Ru_2(Fap)_4(\mu$-CN$)_2$ (**7**) and there is no trace of **6**. The reaction between (4,0) $Ru_2(ap)_4Cl$ and NaCN yields $Ru_2(ap)_4(CN)$ (major) and $Ru_2(ap)_4(CN)_2$ (minor) while the reaction between (4,0) $Ru_2(CH_3ap)_4Cl$ and NaCN yields only the monocyano adduct, $Ru_2(CH_3ap)_4(CN)$ (see Table 2). Thus the mono- and/or dicyano adducts appear as the only products of the reaction that can be isolated from the reaction mixture when the starting materials exist in a (4,0) isomeric form. Indeed, a reaction between the (3,1) isomer of $Ru_2(F_5ap)_4Cl$ and excess NaCN[20] is known to produce only the three edge-sharing diruthenium complexes, $Ru_2(F_5ap)_3[\mu$-(*o*-NC)F_4ap$](\mu$-CN) and $Ru_2(F_5ap)_4(\mu$-CN$)_2$ (two isomers) (see Table 2). The present work shows that the (3,1) isomer also forms mono- and dicyano adducts since both axial cyano adducts and rearranged cyano products are found in the reaction mixture when reacting the (3,1) isomer of $Ru_2(Fap)_4Cl$ with CN^-. The summary of products formed in Table 2 also implies that mono- and/or dicyano adducts of the (3,1) isomers are more likely to be formed when the "ap-type" ligand is more basic. A similar conclusion could also be drawn for the (4,0) isomers (see Table 2), but preliminary data on $Ru_2(F_5ap)_4Cl$ and $Ru_2(3,5\text{-}F_2ap)_4Cl$ indicate that both mono- and dicyano products are also found in the reaction between CN^- and the (4,0) isomers of diruthenium complexes containing an "ap-type" bridging ligand,[33] i.e., F_5ap or 3,5-F_2ap which are both less basic than Fap.

Molecular Structures of Monocyano Complexes 1 and 3. The axially coordinating nature of the cyano ligands in both **1** and **3** were ascertained through single-crystal X-ray diffraction studies. The ORTEPs of **1** and **3** are shown in Figures 1 and 2, respectively, and some selected bond lengths and angles are collected in Table 3. Similar to both the parent compound, $Ru_2(ap)_4Cl$, and the alkynyl analogues, $Ru_2(ap)_4(C_2Y)$,[34−36] ap ligands in the monocyano complexes adopt the (4,0) arrangement where all pyridyl nitrogens (N_p) coordinate to the Ru1 center while all anilino nitrogens (N_a) coordinate to the Ru2 center. The coordination sphere of the Ru1 center can be described as octahedral with Ru2 and CN^- as fifth and sixth ligands while that of Ru2 is square

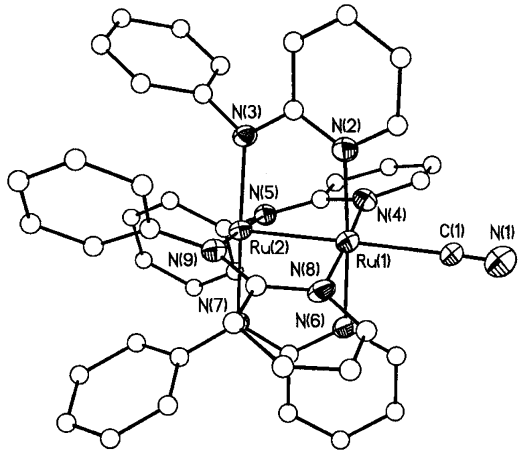

Figure 1. ORTEP diagram of $Ru_2(ap)_4(CN)$ at 30% probability level. H atoms have been omitted for clarity.

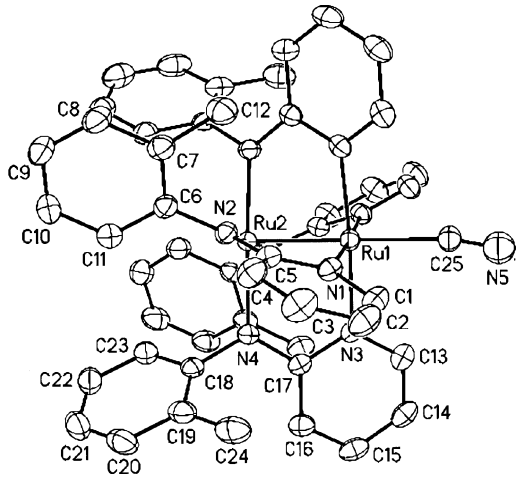

Figure 2. ORTEP plot (40% equiprobability envelopes) of $Ru_2(CH_3ap)_4(CN)$. Hydrogen atoms have been omitted for clarity.

(33) Bear, J. L.; Kadish, K. M.; Van Caemelbecke, E. Manuscript in preparation.

(34) Chakravarty, A. R.; Cotton, F. A.; Tocher, D. A.; Tocher, J. H. *Polyhedron* **1985**, *4*, 1475.
(35) Chakravarty, A. R.; Cotton, F. A. *Inorg. Chim. Acta* **1986**, *113*, 19.
(36) Zou, G.; Alvarez, J. C.; Ren, T. *J. Organomet. Chem.* **2000**, *596*, 152.

Table 3. Selected Bond Lengths (Å) and Angles (deg) for Compounds **1** and **3**

1		**3**	
Ru(1)−N(2)	2.107(6)	Ru(1)−N(1)	2.098(3)
Ru(1)−N(4)	2.111(6)	Ru(1)−N(3)	2.098(3)
Ru(1)−N(6)	2.091(6)	Ru(2)−N(2)	2.056(3)
Ru(1)−N(8)	2.095(6)	Ru(2)−N(4)	2.048(2)
Ru(1)−C(1)	2.210(8)	Ru(1)−C(25)	2.174(5)
Ru(1)−Ru(2)	2.336(2)	Ru(1)−Ru(2)	2.304 (5)
Ru(2)−N(3)	2.041(6)	N(5)−C(25)	1.073(11)
Ru(2)−N(5)	2.037(6)		
Ru(2)−N(7)	2.040(6)		
Ru(2)−N(9)	2.021(6)		
N(1)−C(1)	1.015(10)		
N(2)−Ru(1)−Ru(2)	87.99(18)	N(1)−Ru(1)-Ru(2)	87.83(7)
N(4)−Ru(1)−Ru(2)	88.30(19)	N(3)−Ru(1)-Ru(2)	87.75(7)
N(6)−Ru(1)−Ru(2)	88.74(19)	N(2)−Ru(2)-Ru(1)	89.01(7)
N(8)−Ru(1)−Ru(2)	87.81(18)	N(4)−Ru(2)−Ru(1)	88.88(7)
C(1)−Ru(1)−Ru(2)	178.9(2)	C(25)−Ru(1)−Ru(2)	180
N(3)−Ru(2)−Ru(1)	89.93(18)	N(5)−C(25)−Ru(1)	169(4)
N(5)−Ru(2)−Ru(1)	89.09(18)		
N(7)−Ru(2)−Ru(1)	88.66(18)		
N(9)−Ru(2)−Ru(1)	90.14(18)		
N(1)−C(1)−Ru(1)	177.7(9)		
N(2)−Ru(1)−Ru(2)−N(3)	14.0(2)	N(1)−Ru(1)−Ru(2)−N(2)	21.50(10)
N(4)−Ru(1)−Ru(2)−N(5)	15.5(2)	N(3)−Ru(1)−Ru(2)−N(4)	21.41(10)
N(6)−Ru(1)−Ru(2)−N(7)	16.0(2)		
N(8)−Ru(1)−Ru(2)−N(9)	16.3(2)		

pyramidal. The Ru−Ru bond lengths (2.336(2) Å in **1** and 2.304(5) Å in **3**), while comparable to those in $Ru_2(ap)_4(C_2Y)$ (ca. 2.33 Å),[12] are longer than those of the parent molecule $Ru_2(ap)_4Cl$ (2.275(3) Å), and the elongation is attributed to the strong σ-donor nature of the CN^- ligand in comparison with Cl^-. On the other hand, the Ru−C bond lengths (2.210(8) Å in **1** and 2.174(5) Å in **3**) are significantly longer than the Ru−C distances in $Ru_2(ap)_4(C_2Y)$ type compounds (2.08−2.10 Å),[12] reflecting the weaker basicity of CN^- as compared to an alkynyl ligand. Nevertheless, the similarity in both overall structural features and magnetism implies that compounds **1** and **3** are isoelectronic to other known $Ru_2(ap)_4L_{ax}$ compounds.

While the majority of bond lengths and angles around Ru_2 agree within experimental error with what is seen for **1** and **3**, molecule **3** exhibits a significantly larger N−Ru−Ru′−N′ torsional angle (21.5°) than **1** (15.5°) due to the *o*-methyl substitution on the anilino ring in **3**. Unusually short CN^- bond lengths of 1.015(10) Å (**1**) and 1.073(11) Å (**3**) are also noteworthy, but this feature has previously been reported in dimolybdenum compounds[37] and was attributed to a libration of the crystal structure.[38] While the Ru−Ru−C angle is equal or close to 180° in both molecules, the Ru−C−N angle is still linear in **1** (177.7(9)°) but clearly bent in **3** (169(4)°). The large variance in Ru−C−N angles is likely due to the lack of a significant $Ru_2 \rightarrow \pi^*(CN)$ back-donation.

Molecular Structures of Dicyano Complexes 2 and 5. There are two independent diruthenium molecules (**2A** and **2B**) in the asymmetric unit of crystal **2** but only one in that of **5**. The ORTEPs of **2A** and **5** are shown in Figures 3 and 4, respectively, and the selected bond lengths and angles for molecules **2A**, **2B**, and **5** are listed in Table 4. The Ru−Ru

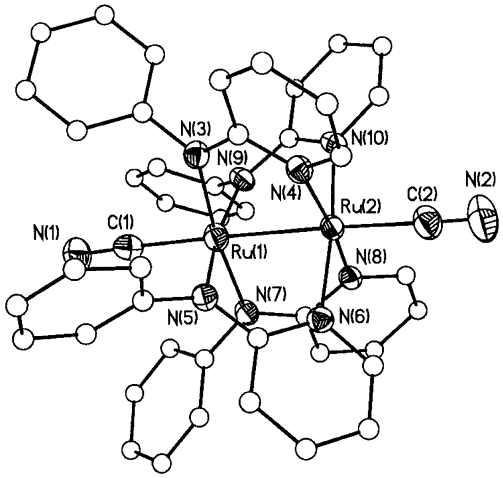

Figure 3. ORTEP diagram of $Ru_2(ap)_4(CN)_2$ at 30% probability level. H atoms have been omitted for clarity.

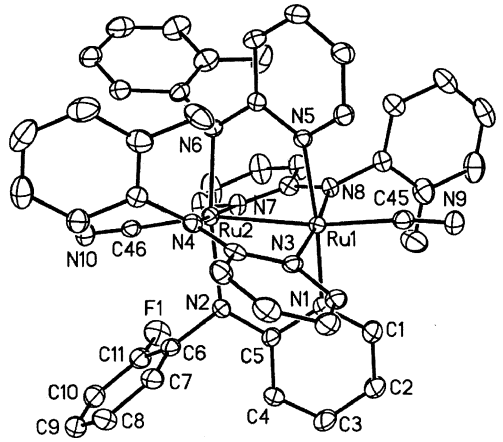

Figure 4. Thermal ellipsoid plot (40% equiprobability envelopes) of the (3,1) isomer of $Ru_2(Fap)_4(CN)_2$. H atoms have been omitted for clarity.

bond lengths, 2.451(3), 2.447(3), and 2.456(5) Å in **2A, 2B**, and **5**, respectively, are identical to each other within experimental error and much longer than the Ru−Ru bonds of **1** and **3** (ca. 2.32 Å). The Ru−C bond lengths in the dicyano adducts (1.99−2.02 Å) are shortened by ca. 0.18 Å from the Ru−C bond lengths of the monocyano adducts. Clearly, the d_{z^2} (Ru) orbital is polarized toward the C center to form a strong σ (Ru−C) bond and is no longer available for Ru−Ru σ-bonding. Evidence corroborating an enhancement of the Ru−C bond in **2** can also be found from the IR data. Both ν_{CN} stretches in **2** are ca. 50 cm^{-1} higher than those found for the monocyano adduct **1**, which is attributed to an enhanced Ru−CN bonding.[39]

Table 4 reveals a peculiar pattern of deviation from the 4-fold symmetry about the Ru_2 core. In the (4,0) molecule **2A**, there are two short $Ru-N_p$ bonds (Ru1−N3 and Ru1−N5 where N_p stands for a pyridyl-nitrogen) and two long $Ru-N_p$ bonds (Ru1−N7 and Ru1−N9) at the "0" site (Ru1), and each short bond is always trans to a long one. The same pattern also holds for $Ru-N_a$ bonds at the "4" site (Ru2) in **2A** (N_a stands for an anilino nitrogen). In the (3,1) molecule **5**, the Ru1 center ("1" site) has two short (Ru1−N1 and

(37) Dunbar, K. R.; Szalay, P. S. *Inorg. Chem. Commun.* **2000**, 49.
(38) Drago, R. S. *Physical Methods in Chemistry*; Saunders: Philadelphia, 1977.
(39) Nakamoto, K. *Infrared and Raman Spectra of Inorganic and Coordination Compounds*, 5th ed.; Wiley: New York, 1997; Vol. B.

Table 4. Selected Bond Lengths (Å) and Angles (deg) for Dicyano Complexes **2** and **5**

2A		2B		5	
Ru(1)−C(1)	2.01(3)	Ru(3)−C(47)	2.03(4)	Ru(1)−N(1)	2.002(4)
Ru(1)−N(3)	2.01(2)	Ru(3)−N(13)	2.00(2)	Ru(1)−N(3)	2.108(3)
Ru(1)−N(5)	2.03(2)	Ru(3)−N(15)	2.12(2)	Ru(1)−N(5)	2.154(3)
Ru(1)−N(7)	2.07(2)	Ru(3)−N(17)	2.06(2)	Ru(1)−N(8)	1.988(4)
Ru(1)−N(9)	2.13(2)	Ru(3)−N(19)	2.04(2)	Ru(1)−C(45)	2.000(5)
Ru(1)−Ru(2)	2.451(3)	Ru(3)−Ru(4)	2.447(3)	Ru(1)−Ru(2)	2.456(5)
Ru(2)−C(2)	2.01(4)	Ru(4)−C(48)	2.02(4)	Ru(2)−N(2)	2.130(4)
Ru(2)−N(4)	2.11(2)	Ru(4)−N(14)	2.11(2)	Ru(2)−N(4)	1.986(3)
Ru(2)−N(6)	2.10(2)	Ru(4)−N(16)	2.06(2)	Ru(2)−N(6)	2.001(3)
Ru(2)−N(8)	2.04(2)	Ru(4)−N(18)	2.05(2)	Ru(2)−N(7)	2.158(3)
Ru(2)−N(10)	2.06(2)	Ru(4)−N(20)	2.10(2)	Ru(2)−C(46)	1.993(5)
N(1)−C(1)	1.17(4)	N(11)−C(47)	1.17(4)	N(9)−C(45)	1.140(6)
N(2)−C(2)	1.13(4)	N(12)−C(48)	1.14(4)	N(10)−C(46)	1.153(6)
N(3)−Ru(1)−Ru(2)	89.5(6)	N(14)−Ru(4)−Ru(3)	83.9(6)	N(1)−Ru(1)−Ru(2)	95.6(1)
N(5)−Ru(1)−Ru(2)	87.5(6)	N(16)−Ru(4)−Ru(3)	89.5(7)	N(3)−Ru(1)−Ru(2)	82.78(9)
N(7)−Ru(1)−Ru(2)	84.0(6)	N(18)−Ru(4)−Ru(3)	89.6(6)	N(5)−Ru(1)−Ru(2)	79.83(9)
N(9)−Ru(1)−Ru(2)	83.5(6)	N(20)−Ru(4)−Ru(3)	84.6(6)	N(8)−Ru(1)−Ru(2)	91.4(1)
C(1)−Ru(1)−Ru(2)	172.8(9)	C(48)−Ru(4)−Ru(3)	171.9(10)	C(45)−Ru(1)−Ru(2)	166.2(1)
N(1)−C(1)−Ru(1)	177(3)	N(11)−C(47)−Ru(3)	177(3)	N(9)−C(45)−Ru(1)	172.7(4)
N(4)−Ru(2)−Ru(1)	83.8(6)	N(13)−Ru(3)−Ru(4)	89.6(7)	N(2)−Ru(2)−Ru(1)	79.20(10)
N(6)−Ru(2)−Ru(1)	84.6(6)	N(15)−Ru(3)−Ru(4)	83.7(6)	N(4)−Ru(2)−Ru(1)	91.01(10)
N(8)−Ru(2)−Ru(1)	89.6(6)	N(17)−Ru(3)−Ru(4)	84.4(6)	N(6)−Ru(2)−Ru(1)	92.39(10)
N(10)−Ru(2)−Ru(1)	89.6(7)	N(19)−Ru(3)−Ru(4)	87.6(6)	N(7)−Ru(2)−Ru(1)	82.69(9)
C(2)−Ru(2)−Ru(1)	171.8(10)	C(47)−Ru(3)−Ru(4)	172.9(9)	C(46)−Ru(2)−Ru(1)	162.5(1)
N(2)−C(2)−Ru(2)	179(4)	N(12)−C(48)−Ru(4)	179(3)	N(10)−C(46)−Ru(2)	176.2(4)
N(3)−Ru(1)−Ru(2)−N(4)	22.5(9)	N(13)−Ru(3)−Ru(4)−N(14)	22.6(9)	N(1)−Ru(1)−Ru(2)−N(2)	15.86(15)
N(5)−Ru(1)−Ru(2)−N(6)	24.8(9)	N(15)−Ru(3)−Ru(4)−N(16)	23.6(9)	N(3)−Ru(1)−Ru(2)−N(4)	19.46(13)
N(7)−Ru(1)−Ru(2)−N(8)	20.8(9)	N(17)−Ru(3)−Ru(4)−N(18)	20.5(9)	N(5)−Ru(1)−Ru(2)−N(6)	24.46(13)
N(9)−Ru(1)−Ru(2)−N(10)	23.7(9)	N(19)−Ru(3)−Ru(4)−N(20)	24.8(8)	N(8)−Ru(1)−Ru(2)−N(7)	18.66(15)

Table 5. Selected Average Bond Lengths (Å) and Bond Angles (deg) of $Ru_2(L)_4(L_{ax})_2$ (L = ap or Fap and L_{ax} = CN or $C_2C_6H_5$)

	(3,1) isomer		(4,0) isomer	
	$Ru_2(Fap)_4(CN)_2$ (**5**)	$Ru_2(Fap)_4(C_2C_6H_5)_2$[a]	$Ru_2(ap)_4(CN)_2$ (**2**)	$Ru_2(ap)_4(C_2C_6H_5)_2$[b]
		bond lengths (Å)		
Ru−Ru	2.456(5)	2.469(6)	2.451	2.4707(3)
Ru−C	1.997(5)	2.002(6)	2.01	1.988(2)
C−N	1.145(6)		1.15	
$Ru-N_a$	2.026(3)	2.020(4)	2.06	2.050(2)
$Ru-N_p$	2.106(4)	2.130(4)	2.08	2.067(3)
		bond angles (deg)		
Ru−Ru−C	164.4(12)	161.0(17)	172.3(9)	163.0(1)
$Ru-Ru-N_a$	88.50(9)	90.33(10)	86.1(6)	85.6(1)
$Ru-Ru-N_p$	85.24(10)	83.08(11)	86.9(6)	87.0(1)
N−Ru−Ru−N	19.6	18.2	22.9	22.4

[a] Reference 41. [b] Reference 42.

Ru1−N8) bonds that are trans to two long (Ru1−N3 and Ru1−N5) bonds. In addition to the disparity among Ru−N distances, average Ru−Ru−C angles in **2** (172.5°) and **5** (164.1°) deviate significantly from linearity. As elaborated for diruthenium dialkynyl complexes, these distortions have an electronic origin, a second-order Jahn−Teller effect.[12,19,30,40] As in the case of the monoadduct, compounds **2** and **5** are isoelectronic with previously characterized $Ru_2(ap)_4(C_2Y)_2$.

X-ray structures of diphenylacetylide analogues of **2** and **5** were previously reported,[41,42] and some relevant bond lengths and angles are gathered in Table 5 along with those of **2** and **5** for comparison purpose.

Molecular Structure of Compound 8. The molecular structure of **8** is given in Figure 5 while Table 6 summarizes selected averaged bond lengths and bond angles of **8** along with those of $Ru_2(F_5ap)_3[\mu\text{-}(o\text{-NC})F_4ap)](\mu\text{-CN})$[20] for comparison purposes. Compound **8** and previously characterized $Ru_2(F_5ap)_3[\mu\text{-}(o\text{-NC})F_4ap)](\mu\text{-CN})$[20] possess a similar coordination sphere around the Ru_2 core. These two compounds also exhibit similar bond lengths and bond angles (Table 6) despite the fact that F_5ap is more bulky and more electron withdrawing than the F_3ap ligand. In both cases, the coordination sphere of the two Ru atoms can be described as a distorted octahedral with Ru1 attached to three N_p and one N_a centers and Ru2 attached to one N_p and three N_a centers. The edge-sharing motif is completed with the two octahedrons fusing along a common equatorial edge defined by C45 and C46 centers. Two of the F_3ap ligands are chelated to Ru centers, while the other two are in three-atom bidentate bridging modes. The Ru−Ru bond length of **8** (see Table 6) is similar to that of $Ru_2(F_5ap)_3[\mu\text{-}(o\text{-NC})F_4ap)](\mu\text{-CN})$[20] but is 0.36 Å longer than its parent compound $Ru_2(F_3ap)_4Cl$.[24] The elongation of the bond is consistent with a decrease in

(40) Lin, C.; Ren, T.; Valente, E. J.; Zubkowski, J. D. *J. Chem. Soc., Dalton Trans.* **1998**, 571.
(41) Wellhoff, J. M.S. Thesis, University of Houston, Houston, TX, 2000.
(42) Huang, S. R. Ph.D. Dissertation, University of Houston, Houston, TX, 1994.

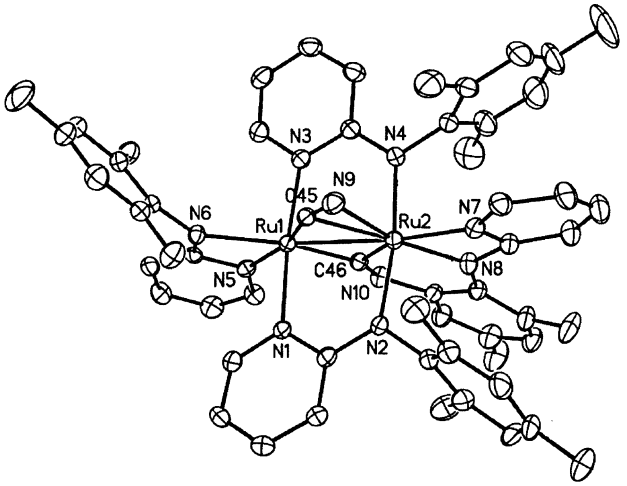

Figure 5. Thermal ellipsoid plot (40% equiprobability envelopes) of the (3,1) isomer of $Ru_2(F_3ap)_3[\mu\text{-}(o\text{-}CN)F_2ap](\mu\text{-}CN)$. H atoms have been omitted for clarity.

Table 6. Selected Average Bond Lengths (Å) and Bond Angles (deg) of $Ru_2(F_xap)_3[\mu\text{-}(o\text{-}NC)F_{x-1}ap)](\mu\text{-}CN)$ ($x = 3$ or 5)

	$x = 3$	$x = 5$[a]
	bond lengths (Å)	
Ru−Ru	2.644	2.647
Ru−C(45)	2.086	1.980
Ru−C(46)	1.986	1.988
C(45)−N(9)	1.174	1.173
C(46)−N(10)	1.232	1.227
$Ru-N_a$	2.057	2.063
$Ru-N_p$	2.092	2.102
	bond angles (deg)	
Ru(1)−C(45)−N(9)	163.0	161.6
C(46)−N(10)−C(44)	143.3	142.6
$Ru-Ru-N_a$	114.9	114.5
$Ru-Ru-N_p$	119.8	120.3

[a] Reference 20.

bond order (b.o.) upon going from (3,1) $Ru_2(F_3ap)_4Cl$ (b.o. = 2.5) to **8** (b.o. = 0.5). Also, in general, the averaged Ru(1)−N bond distance is 0.27 Å longer than the averaged Ru(2)−N distance and this was also the case for $Ru_2(F_5ap)_3[\mu\text{-}(o\text{-}NC)F_4ap)](\mu\text{-}CN)$.[20]

As previously discussed for $Ru_2(F_5ap)_3[\mu\text{-}(o\text{-}NC)F_4ap)](\mu\text{-}CN)$, the C45−N9 cyanide ligand is σ-bonded to Ru(1) and π-bonded to Ru(2), resulting in an asymmetry of the bridging cyanide ligand.[20] This phenomenon is also seen in **8** where the C45−N9 cyanide ligand bridges two ruthenium atoms. In addition, the Ru1−C45−N9 angle of 163.0° (see Table 6) also suggests that the cyanide group of $Ru_2(F_3ap)_3[\mu\text{-}(o\text{-}NC)F_2ap)](\mu\text{-}CN)$ bridges the two ruthenium atoms in a $\sigma-\pi$ mode. Similar to the case of the F_5ap derivative, the bond length of C(45)−N(9) (1.174 Å) is slightly shorter than that of C(46)−N(10) (1.232 Å). The $\sigma-\pi$ binding modes of CN^- are consistent with the low frequency of CN^- vibrations (less than 2000 cm^{-1}), the latter of which are influenced by π back-donation from the Ru_2 dimetal core.[7,39]

Electrochemistry of $Ru_2(L)_4(CN)_x$ (L = ap or Fap). The three investigated mono-CN complexes, which are in a Ru_2^{5+} oxidation state in their air-stable form, undergo one reduction and two oxidations, while the two dicyano species, which contain a Ru_2^{6+} core, are characterized by two reductions and one oxidation. Each electrochemical process is proposed to involve the dimetal unit. The half-wave potentials in CH_2Cl_2, 0.1 M TBAP are given in Table 7, and cyclic voltammograms for $Ru_2(Fap)_4(CN)$ and $Ru_2(Fap)_4(CN)_2$ are shown in Figure 6. The $Ru_2^{6+/5+}$ and $Ru_2^{5+/4+}$ couples of $Ru_2(Fap)_4(CN)_2$ are located at $E_{1/2} = -0.21$ and -1.08 V and are both negatively shifted with respect to the same electrode reactions of $Ru_2(Fap)_4(CN)$ ($E_{1/2} = 0.52$ and -0.68 V). The largest shift is seen for the $Ru_2^{6+/5+}$ process ($\Delta E_{1/2} = 730$ mV) while the smallest (400 mV) is seen for $Ru_2^{5+/4+}$.

Table 7. Half-Wave Potentials (V vs SCE) for Redox Processes of $Ru_2(L)_4(L_{ax})_n$ (L = ap, CH_3ap, or Fap; L_{ax} = Cl or CN; and $n = 1$ or 2) in CH_2Cl_2 Containing TBAP as Supporting Electrolyte

isomer type	bridging ligand, L	axial ligand, L_{ax}	$E_{1/2}$, V vs SCE $Ru_2^{7+/6+}$	$Ru_2^{6+/5+}$	$Ru_2^{5+/4+}$	ref
(4,0)	ap	Cl^-		0.37	−0.86	42
		CN^-	1.30	0.43	−0.73	*b*
		2 CN^-	1.02[a]	−0.24	−1.24[a]	*b*
(4,0)	CH_3ap	Cl^-	1.44	0.41	−0.89	24
		CN^-	1.08[a]	0.46	−0.73	*b*
(3,1)	Fap	Cl^-	1.43	0.47	−0.77	25
		CN^-	1.47	0.52	−0.68	*b*
		2 CN^-	0.92	−0.21	−1.08	*b*

[a] E_p at 0.1 V/s. [b] This work.

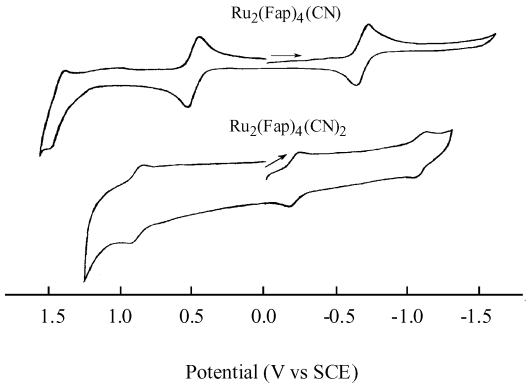

Figure 6. Cyclic voltammograms of $Ru_2(Fap)_4(CN)$ and $Ru_2(Fap)_4(CN)_2$ in CH_2Cl_2 containing 0.1 M TBAP. Scan rate = 0.1 V/s.

A similar trend in $E_{1/2}$ is seen when comparing the $Ru_2^{6+/5+}$ and $Ru_2^{5+/4+}$ couples of $Ru_2(ap)_4(CN)$ (Figure 7) and $Ru_2(ap)_4(CN)_2$ (Figure 8), but $Ru_2(ap)_4(CN)_2$ is less stable than $Ru_2(Fap)_4(CN)_2$ in CH_2Cl_2 and undergoes a loss of one CN^- ligand to give a mixture of $[Ru_2^{III,III}(ap)_4(CN)]^+$ and $Ru_2^{III,III}(ap)_4(CN)_2$ in solution, prior to carrying out the experiment. This is evident from Figure 8, which shows a reversible process at $E_{1/2} = -0.73$ V, which also appears in the cyclic voltammogram of $Ru_2(ap)_4(CN)$ (see Figure 7).

This reaction sequence of $Ru_2(ap)_4(CN)_2$ is given in Scheme 3 where the process at $E_{1/2} = -0.73$ V corresponds to the reduction of $Ru_2(ap)_4(CN)$ and that at -0.29 and -1.25 V correspond to the electrode reaction of $Ru_2(ap)_4(CN)_2$.

As seen in Figure 8, the two reduction processes of the dicyano adduct have larger currents than the single reduction in the case of the monocyano adduct, thus indicating that $Ru_2(ap)_4(CN)_2$ is the predominant species in solution under these experimental conditions. The third reduction in Figure 8 (the second reduction of $Ru_2(ap)_4(CN)_2$) is irreversible and is accompanied by an increased formation of $[Ru_2(ap)_4(CN)]^-$.

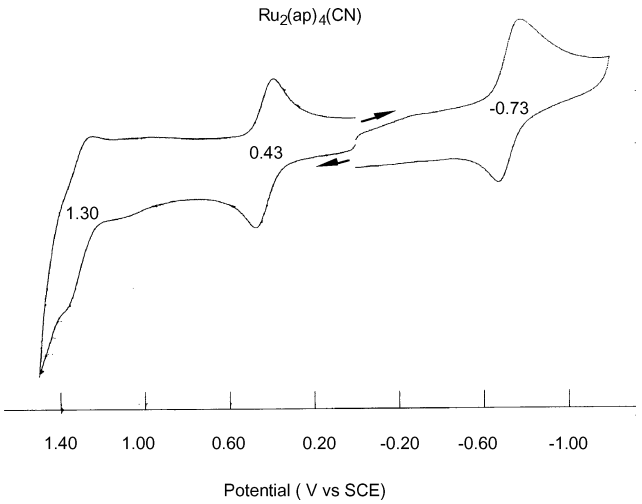

Figure 7. Cyclic voltammogram of $Ru_2(ap)_4(CN)$ in CH_2Cl_2 containing 0.1 M TBAP at a scan rate of 0.1 V/s.

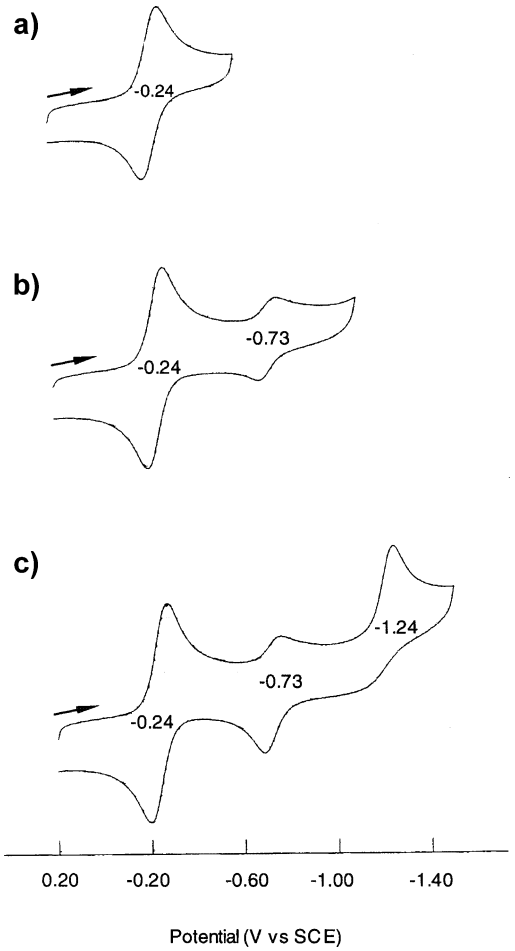

Figure 8. Cyclic voltammogram of $Ru_2(ap)_4(CN)_2$ in CH_2Cl_2 containing 0.1 M TBAP after reversing the scan after (a) the first, (b) the second, and (c) the third reduction. Scan rate = 0.1 V/s.

Thus, the reoxidation currents for the process at −0.73 V are larger than those obtained when the potential is terminated at −1.00 V. This is shown in Figure 8c.

As seen in Table 7, the reduction of each "ap-type" complex shifts in a positive direction upon switching the axial ligand from Cl^- to CN^-, with the magnitude of the potential shift ranging from 90 mV for the ap and Fap derivatives to

Scheme 3

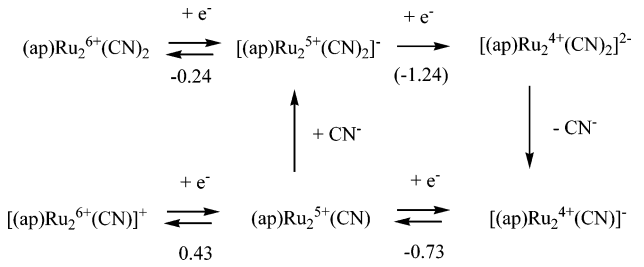

160 mV for the CH_3ap derivative. This is because the π-backbonding effect (which results from a good overlap between the π^*_{Ru-Ru} orbital and the empty π^*_{CN} orbital) between CN^- and the dimetal core stabilizes the Ru_2^{4+} oxidation state of each compound. There is only a small effect of the axial ligand on the oxidation of the compounds, thus revealing that the lowest unoccupied molecular orbital (LUMO) is more sensitive to axial ligation than the highest occupied molecular orbital (HOMO), a result consistent with the fact that the reduction of $Ru_2(L)_4Cl$ (L = ap, Fap, or CH_3ap) has been proposed to involve the π^* orbital while the oxidation the δ^* orbital.[24]

Electrochemical and Spectroscopic Properties of $Ru_2(F_xap)_3[\mu\text{-}(o\text{-NC})F_{x-1}ap](\mu\text{-CN})$ (x = 1, 3, or 5). Figure 9 illustrates cyclic voltammograms of $Ru_2(F_xap)_3[\mu\text{-}(o\text{-NC})F_{x-1}ap)](\mu\text{-CN})$ (x = 1, 3, or 5) in CH_2Cl_2 containing 0.1 M TBAP. Each redox reaction of the compounds in Table 8 (labeled as I, II, and III in Figure 9) shifts in a cathodic direction upon going from x = 5 to x = 1, and this is attributed to a higher electronic density of the diruthenium core owing to a decrease in the electron-withdrawing properties of the equatorial bridging ligands. A similar trend was reported in the case of $Ru_2(F_xap)_4Cl$ (x = 0, 1, 3, or 5) where the data were analyzed in terms of LFER between $E_{1/2}$ and $\Sigma\sigma$ for the substituents on the anilino part of the bridging ligand.[24] In fact, similar correlations between $E_{1/2}$ and $\Sigma\sigma$ exist for the three redox reactions of $Ru_2(F_xap)_3[\mu\text{-}(o\text{-NC})F_{x-1}ap)](\mu\text{-CN})$ (x = 1, 3, or 5) as shown in Figure 10. The correlation coefficients (R^2) for the $E_{1/2}$ vs $\Sigma\sigma$ plots in Figure 10 are 0.996 for the first reduction and 0.999 for both oxidations and the fact that the plots give good fits suggests that **6** should indeed be formulated as $Ru_2(Fap)_3[\mu\text{-}(o\text{-NC})ap)](\mu\text{-CN})$, although no X-ray crystal structure could be obtained to confirm this structure. The first reduction of $Ru_2(F_xap)_3[\mu\text{-}(o\text{-NC})F_{x-1}ap)](\mu\text{-CN})$ exhibits a ρ value of 108 mV and this is virtually the same as what is seen for the first oxidation where ρ = 111 mV, thus suggesting that the electron is added or removed from the same orbital. This is indeed the case as discussed in the next paragraph.

The well-resolved ESR spectrum of $Ru_2(F_3ap)_3[\mu\text{-}(o\text{-NC})F_2ap)](\mu\text{-CN})$ (**8**) shows a rhombic signal with three g values (g_1 = 2.118, g_2 = 2.042, g_3 = 1.944) and resembles the ESR spectra[19,20,43] of $Ru_2(F_5ap)_3[\mu\text{-}(o\text{-NC})F_4ap)](\mu\text{-CN})$, $[Ru_2(F_5ap)_4(C{\equiv}CC_6H_5)_2]^-$, and $[Ru_2(dpf)_4(C{\equiv}CC_6H_5)_2]^-$, all of which

(43) Bear, J. L.; Li, Y.; Han, B.; Van Caemelbecke, E.; Kadish, K. M. *Inorg. Chem.* **1997**, *36*, 5449.

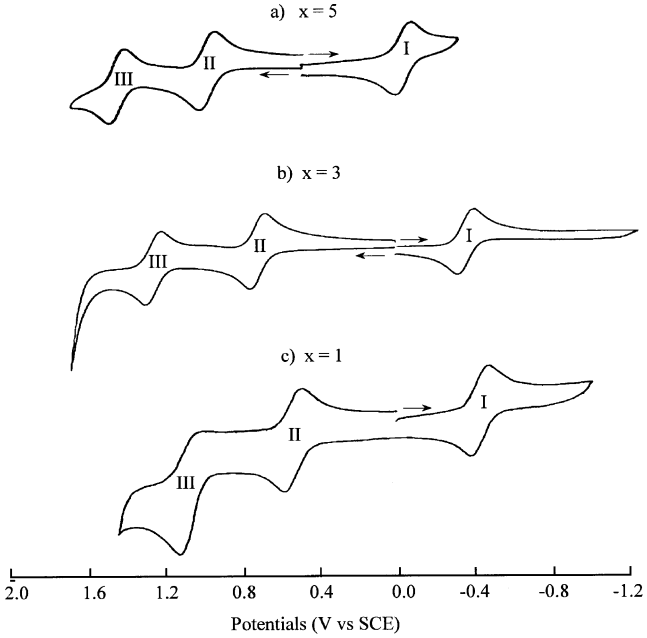

Figure 9. Cyclic voltammograms of $Ru_2(F_xap)_3[\mu\text{-}(o\text{-}NC)F_{x-1}ap](\mu\text{-}CN)$ ($x = 1$, 3 or 5) in CH_2Cl_2 containing 0.1 M TBAP. Scan rate = 0.1 V/s.

Table 8. Half-Wave Potentials (V vs SCE) of $Ru_2(F_xap)_3[\mu\text{-}(o\text{-}NC)F_{x-1}ap](\mu\text{-}CN)$ ($x = 1$, 3, or 5) in CH_2Cl_2 Containing 0.1 M TBAP

		oxidation		reduction
		Ru_2^{7+}/Ru_2^{6+}	Ru_2^{6+}/Ru_2^{5+}	Ru_2^{5+}/Ru_2^{4+}
x	$4\Sigma\sigma^a$	(III)	(II)	(I)
5	4.64	1.45	0.96	−0.01
3	1.92	1.20	0.68	−0.32
1	0.72	1.08	0.52	−0.43

[a] Because one of the F atoms on the chelating F_xap ligand is substituted by one of the bridging cyanides, the value of $\Sigma\sigma^b$ was calculated based on only three fluorine atoms on the ligand. [b] Zuman, P. *Substituent Effects in Organic Polarography*; Plenum Press: New York, 1967.

have been assigned as diruthenium(II,III) complexes. The magnetic susceptibility of **8** was calculated using the Evan's method and the room temperature magnetic moment of 1.45 μB is consistent with the presence of only one unpaired electron in the compound. On the basis of the ESR and magnetic properties, **8** is therefore proposed to have the electronic configuration $\sigma^2\pi^2\delta^2\delta^{*2}\pi^{*2}\sigma^{*1}$. The same electronic structure was given to $Ru_2(F_5ap)_3[\mu\text{-}(o\text{-}NC)F_4ap)](\mu\text{-}CN)$,[20] a compound with a similar structural type and whose ESR features and magnetic properties resemble what is seen in the case of **8**. This electronic configuration implies that the HOMO and LUMO are both the σ^* orbital, thus resulting in virtually the same ρ value for the first reduction and the first oxidation of the series $Ru_2(F_xap)_3[\mu\text{-}(o\text{-}NC)F_{x-1}ap)](\mu\text{-}CN)$ ($x = 1$, 3, or 5) as shown in Figure 10.

Proposed Mechanism of Rearrangement. Table 2 shows that when the product formulated as $Ru_2(F_xap)_3[\mu\text{-}(o\text{-}NC)F_{x-1}ap)](\mu\text{-}CN)$ ($x = 1$ or 5) is obtained in the reaction between CN^- and $Ru_2(F_xap)_4Cl$, the reaction mixture also contains one or two additional compounds with the structural type $Ru_2(F_xap)_4(\mu\text{-}CN)_2$. This is most likely also true for $Ru_2(F_3ap)_4Cl$ (although as discussed in the Experimental Section all products of the reaction were not isolated and

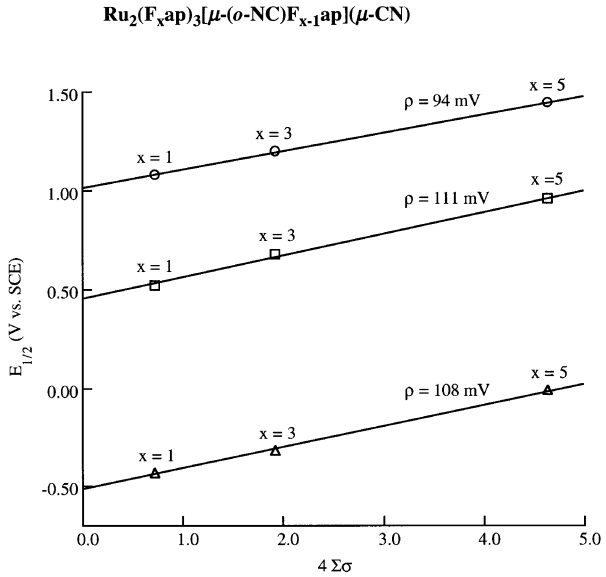

Figure 10. Linear free energy relationship for the redox reactions of the (3,1) isomer of $Ru_2(F_xap)_3[\mu\text{-}(o\text{-}NC)F_{x-1}ap](\mu\text{-}CN)$ ($x = 1$, 3 or 5) (open circle: second oxidation, open square: first oxidation and open triangle: first reduction).

characterized) since the purification of the reaction mixture reveals that $Ru_2(F_3ap)_3[\mu\text{-}(o\text{-}NC)F_2ap)](\mu\text{-}CN)$ is not the only product formed during the reaction.

The direct precursor of $Ru_2(F_5ap)_3[\mu\text{-}(o\text{-}NC)F_4ap)](\mu\text{-}CN)$ has been identified as one of the two geometric isomers of $Ru_2(F_5ap)_4(\mu\text{-}CN)_2$,[20] and the formation of $Ru_2(F_xap)_4(\mu\text{-}CN)_2$ ($x = 1$ or 3) appears therefore to be the key step in the overall conversion of $Ru_2(F_xap)_4Cl$ to $Ru_2(F_xap)_3[\mu\text{-}(o\text{-}NC)F_{x-1}ap)](\mu\text{-}CN)$.

As shown in Scheme 4, three different routes can be proposed for the formation of $Ru_2(F_xap)_4(\mu\text{-}CN)_2$ (b). First of all, the reaction product (b) could be simply a rearrangement of the reaction product (a) (see route 2 in Scheme 4) due to a preferred electronic configuration or a more thermodynamically stable structure (although no experimental data has yet been obtained to support this mechanism). Routes 1 and 3 can also be proposed for formation of reaction product (b) but it is not clear at this time how a second CN^- ligand can be added to the monocyano product $Ru_2(F_xap)_4(CN)$ or $[Ru_2(F_xap)_4(CN)Cl]^-$ without forming the dicyano adduct $Ru_2(F_xap)_4(CN)_2$ as an intermediate. One possibility is that the monocyano adduct undergoes a structural rearrangement prior to addition of a second ligand, but no trace of such a product has yet been found in the reaction mixture.

Summary

In the present study, we have structurally and electrochemically examined the products of the reaction between CN^- and four different diruthenium complexes of the type $Ru_2(L)_4Cl$ where L is ap or a substituted ap ligand. The type of reaction products varies with the nature of the bridging ligand and in some cases with the experimental conditions themselves. More specifically, only mono- and/or dicyano adducts are found as reaction products when L = ap or CH_3-ap but compounds with the structural type $Ru_2(F_xap)_3[\mu\text{-}(o\text{-}NC)F_{x-1}ap](\mu\text{-}CN)$ or $Ru_2(F_xap)_4(\mu\text{-}CN)_2$ are also isolated

Scheme 4

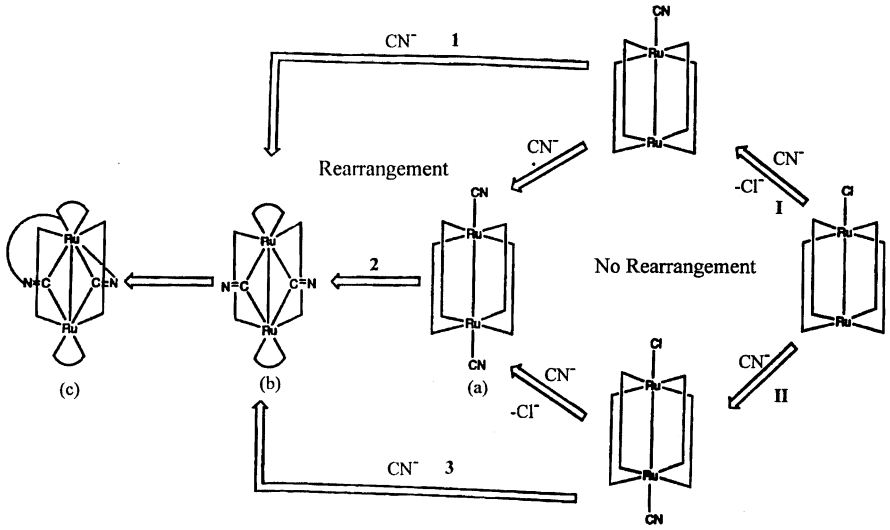

when L = Fap or F_3ap. Interestingly, the reaction between CN^- and the (3,1) isomer of $Ru_2(L)_4Cl$ where L is an "ap-type" ligand is more likely to form a mono- or dicyano adduct as the basicity of the bridging ligand increases. Both mono- and dicyano derivatives possess the isomer type of their parent chloro complexes, but Ru−Ru bond lengths in the monocyano derivatives are larger than those in their respective chloro derivatives owing to the strong σ-donor properties of the CN^- axial ligand. The crystal structure and the IR data of $Ru_2(ap)_4(CN)_2$ reveal a greatly enhanced interaction between the CN group and the dimetal core in the dicyano complex. All synthesized mono- and dicyano adducts were also electrochemically investigated in CH_2Cl_2. $Ru_2(ap)_4(CN)$, $Ru_2(CH_3ap)_4(CN)$, and $Ru_2(Fap)_4(CN)$ exhibit a similar behavior, and the three compounds undergo one reversible reduction and two oxidations within the solvent potential range investigated.

Acknowledgment. This work is supported in part by both the University of Miami and the Petroleum Research Fund/ACS (36595-AC3). The support of the Robert A. Welch Foundation (J.L.B., Grant E-918; K.M.K., Grant E-680) is also gratefully acknowledged. We thank Dr. J. D. Korp for performing the X-ray analyses as well as Tuan Phan and Dr. Giribabu for help in electrochemical measurements.

Supporting Information Available: X-ray crystallographic files in CIF format for the structure determination of compounds **1**−**3**, **5** and **8**. This material is available free of charge via the Internet at http://pubs.acs.org.

IC030195M